

# LUMINOSITY AND CLUSTERING OF GALAXIES SELECTED BY EW (H $\alpha$ )

J. Loveday <sup>1</sup>, L. Tresse <sup>2</sup>, S.J. Maddox <sup>3</sup>

<sup>1</sup> *Astronomy and Astrophysics, University of Chicago, Chicago, USA.*

<sup>2</sup> *Istituto di Radioastronomia del CNR, Bologna, Italia.*

<sup>3</sup> *Institute of Astronomy, Cambridge, UK.*

## Abstract

We study the luminosity function and clustering properties of subsamples of local galaxies selected from the Stromlo-APM survey by the rest-frame equivalent width (EW) of the H $\alpha$  emission line. The  $b_J$  luminosity function of star-forming galaxies has a significantly steeper faint-end slope than that for quiescent galaxies: the majority of sub- $L^*$  galaxies are currently undergoing significant star formation. Emission line galaxies are less strongly clustered, both amongst themselves, and with the general galaxy population, than quiescent galaxies. Thus as well as being less luminous, star-forming galaxies also inhabit lower-density regions of the Universe than quiescent galaxies.

## 1 Galaxy Samples

Our sample of galaxies is taken from the Stromlo-APM redshift survey which covers 4300 sq-deg of the south galactic cap and consists of 1797 galaxies brighter than  $b_J = 17.15$  mag. The galaxies all have redshifts  $z < 0.145$ , and the mean is  $\langle z \rangle = 0.051$ . A detailed description of the spectroscopic observations and the redshift catalog is published in [7]. Measurement of EW (H $\alpha$ ) and other spectral properties is described in [11] and a more detailed analysis of the luminosity function and clustering of galaxies selected by EW (H $\alpha$ ) as well as EW ([O II]) may be found in [8]. Of the 1797 galaxies originally published in the redshift survey, 1521 are suitable for analysis here. The rest are brighter than 15th magnitude, and so have unreliable APM photometry, or have a problem with the spectrum meaning that EW (H $\alpha$ ) could not be accurately measured.

We select galaxy subsamples using measured equivalent width of the H $\alpha$  emission line, the most reliable tracer of massive star formation [2]. The H $\alpha$  line is detected with  $\text{EW} \geq 2\text{\AA}$  in 61% of galaxies. Of these emission-line galaxies, half have  $\text{EW} (\text{H}\alpha) > 15\text{\AA}$ . Thus we form three subsamples of comparable size by dividing the sample at EW (H $\alpha$ ) of  $2\text{\AA}$  and  $15\text{\AA}$ . The galaxy samples selected by H $\alpha$  equivalent width are defined in Table 1 which also gives the numbers of galaxies of each morphological type in each spectroscopically selected subsample. The sample labeled “Unk” consists of galaxies to which no morphological classification was assigned. We see that early-type galaxies dominate when H $\alpha$  emission is not detected and are underrepresented when emission is detected. Conversely, the number of irregular galaxies increases significantly in the spectroscopic samples which show strongest star formation.

Table 1: Spectroscopic subsamples and correlation with morphological type.

Sample	EW (H $\alpha$ )	E	S0	Sp	Irr	Unk	Total
(a) H-low	< 2 Å	125	108	207	10	149	599
(b) H-mid	2–15 Å	8	16	340	18	81	463
(c) H-high	> 15 Å	11	9	303	41	95	459

## 2 The Galaxy Luminosity Function

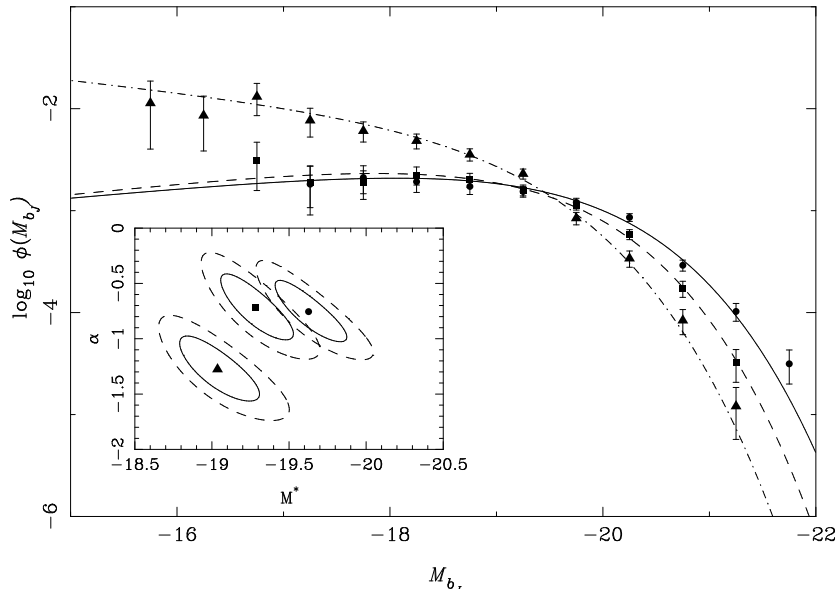


Figure 1: Estimates of the luminosity function for galaxies with no significant detected H $\alpha$  emission (H-low: circles, solid line), with moderate H $\alpha$  emission (H-mid: squares, dashed line) and with strong H $\alpha$  emission (H-high: triangles, dot-dashed line). The symbols with error bars show a stepwise fit, the curves show Schechter function fits. For clarity, data points representing fewer than five galaxies have been omitted from the plot. The inset shows 1 & 2 $\sigma$  likelihood contours for the best-fit Schechter parameters.

Our estimates of the luminosity function for the EW (H $\alpha$ ) selected samples, assuming a Hubble constant of  $H_0 = 100$  km/s/Mpc, are shown in Figure 1. The inset to this Figure shows the likelihood contours for the best-fit Schechter parameters  $\alpha$  and  $M^*$ . The Schechter parameters and their  $1\sigma$  errors (from the bounding box of the  $1\sigma$  error contours) are also listed in Table 2. Note that the estimates of  $\alpha$  and  $M^*$  are strongly correlated and so the errors quoted for  $\alpha$  and  $M^*$  in the Table are conservatively large. We see a trend of faintening  $M^*$  and steepening  $\alpha$  as EW (H $\alpha$ ) increases.

The normalisation  $\phi^*$  of the fitted Schechter functions was estimated using a minimum variance estimate of the space density  $\bar{n}$  of galaxies in each sample [1], [5]. We corrected our estimates of  $\bar{n}$ ,  $\phi^*$  and luminosity density  $\rho_L$  to allow for those galaxies excluded from each subsample. The uncertainty in mean density due to “cosmic variance” is  $\approx 6\%$  for each sample. However, the errors in these quantities are dominated by the uncertainty in the shape of the LF, particularly by the estimated value of the characteristic magnitude  $M^*$ .

Using H $\alpha$  equivalent width as an indicator of star formation activity, we find that galaxies currently undergoing significant bursts of star formation dominate the faint-end of the luminosity function, whereas more quiescent galaxies dominate at the bright end. This is in agreement

Table 2: Luminosity and correlation function parameters.

Sample	$\alpha$	$M^*$	$\phi^*$	$\rho_L$	$\gamma$	$r_0$
(a) H-low	$-0.75 \pm 0.28$	$-19.63 \pm 0.24$	$4.5 \pm 1.1$	$5.9 \pm 1.4$	$1.78 \pm 0.08$	$6.0 \pm 1.4$
(b) H-mid	$-0.72 \pm 0.29$	$-19.28 \pm 0.23$	$5.4 \pm 1.4$	$5.1 \pm 1.4$	$1.60 \pm 0.13$	$5.2 \pm 2.0$
(c) H-high	$-1.28 \pm 0.30$	$-19.04 \pm 0.26$	$8.5 \pm 2.8$	$8.8 \pm 2.9$	$1.87 \pm 0.16$	$2.9 \pm 1.9$

Notes:  $\alpha$  is the faint-end slope and  $M^*$  the characteristic  $b_J$  magnitude of the best-fit Schechter function.  $\phi^*$  is the normalisation of the Schechter luminosity function, in units of  $10^{-3}h^3\text{Mpc}^{-3}$ .  $\rho_L$  is the luminosity density in the range  $-22 < M < -15$ , in units of  $10^7L_\odot h^3\text{Mpc}^{-3}$ .  $\gamma$  and  $r_0$  are the best-fit power-law parameters to the correlation function.

with the results from the LCRS [4] and ESP [12] surveys for samples selected by EW ([O II]).

### 3 Galaxy Clustering

We have calculated the projected cross-correlation function  $\Xi(\sigma)$  of each galaxy subsample with all galaxies in the APM survey to a magnitude limit of  $b_J = 17.15$ . We then invert this projected correlation function to obtain the real space cross-correlation function  $\xi(r)$  of each subsample with the full galaxy sample. This method of estimating  $\xi(r)$  is described by [9] and by [6]. Our estimates of  $\xi(r)$  are plotted in Figure 2 and our best-fit power-laws are tabulated in Table 2. We see that strong emission-line galaxies are more weakly clustered than their quiescent counterparts by a factor of about two.

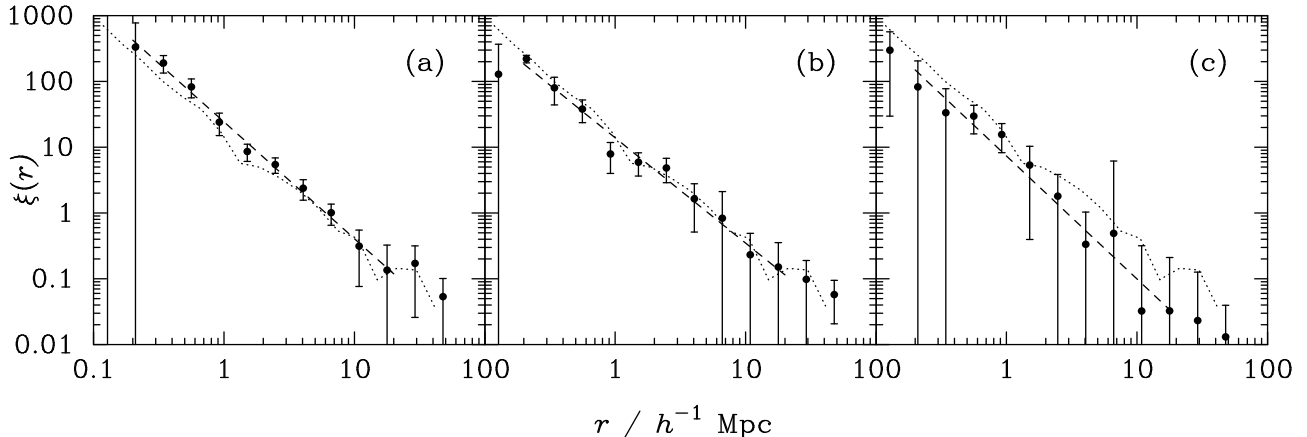


Figure 2: Estimates of the real-space correlation function for the galaxy samples given in Table 1. Error bars show the rms variance from dividing the survey into 4 distinct zones. The dashed line shows the best-fit power-law over the range  $0.2\text{--}20 h^{-1}\text{Mpc}$ . The dotted line shows  $\xi(r)$  estimated from the full Stromlo-APM sample [6].

The clustering measured for non-ELGs is very close to that measured for early-type (E + S0) galaxies, and the clustering of late-type (Sp + Irr) galaxies lies between that of the moderate and high EW galaxies (cf. [6]). Given the strong correlation between morphological type and presence of emission lines (Table 1) this result is not unexpected. The power-law slopes are consistent ( $\gamma_r = 1.8 \pm 0.1$ ) between the H-low and H-high samples. For the H-mid sample we find shallower slopes ( $\gamma_r = 1.6 \pm 0.1$ ). This is only a marginally significant ( $1\text{--}2 \sigma$ ) effect, but may indicate a deficit of moderately star-forming galaxies principally in the cores

of high density regions, whereas strongly star forming galaxies appear to more generally avoid overdense regions.

## 4 Conclusions

We have presented the first analysis of the luminosity function and spatial clustering for representative and well-defined local samples of galaxies selected by  $\text{EW}(\text{H}\alpha)$ , the most direct tracer of star-formation. We observe that  $M^*$  faintens systematically with increasing  $\text{EW}(\text{H}\alpha)$ , and that the faint-end slope increases. Star-forming galaxies are thus likely to be significantly fainter than their quiescent counterparts. The faint-end ( $M \gtrsim M^*$ ) of the luminosity function is dominated by ELGs and thus the majority of local dwarf galaxies are currently undergoing star formation. Star-forming galaxies are more weakly clustered than quiescent galaxies. This weaker clustering is observable on scales from  $0.1\text{--}10 h^{-1}\text{Mpc}$ . We thus confirm that star-forming galaxies are preferentially found today in low-density environments.

A possible explanation for these observations is that luminous galaxies in high-density regions have already formed all their stars by today, while less luminous galaxies in low-density regions are still undergoing star formation. It is not clear what might be triggering the star formation in these galaxies today. While interactions certainly enhance the rate of star formation in some disk galaxies, interactions with luminous companions can only account for a small fraction of the total star formation in disk galaxies today ([3]). Telles & Maddox [10] have investigated the environments of H II galaxies by cross-correlating a sample of H II galaxies with APM galaxies as faint as  $b_J = 20.5$ . They find no excess of companions with H I mass  $\gtrsim 10^8 M_\odot$  near H II galaxies, thus arguing that star formation in most H II galaxies is unlikely to be induced by even a low-mass companion.

Our results are entirely consistent with the hierarchical picture of galaxy formation. In this picture, today's luminous spheroidal galaxies formed from past mergers of galactic sub-units in high density regions, and produced all of their stars in a merger induced burst, or series of bursts, over a relatively short timescale. The majority of present-day dwarf, star-forming galaxies in lower density regions may correspond to unmerged systems formed at lower peaks in the primordial density field and whose star formation is still taking place. Of course, the full picture of galaxy formation is likely to be significantly more complicated than this simple sketch, and numerous physical effects such as depletion of star-forming material and other feedback mechanisms are likely to play an important role.

## References

- [1] Davis, M. & Huchra, J., 1982, ApJ, 254, 437
- [2] Kennicutt, R.C. 1983, ApJ, 272, 54
- [3] Kennicutt, R.C., Keel, W.C., van der Hulst, J.M., Hummel, E. & Roettiger, K.A., 1987, AJ, 93, 1011
- [4] Lin, H., et al., 1996, ApJ, 464, 60
- [5] Loveday, J., Peterson, B.A., Efstathiou, G. & Maddox, S.J., 1992, ApJ, 390, 338
- [6] Loveday, J., Maddox, S.J., Efstathiou, G., & Peterson, B.A., 1995, ApJ, 442, 457
- [7] Loveday, J., Peterson, B.A., Maddox, S.J., & Efstathiou, G., 1996, ApJS, 107, 201
- [8] Loveday, J., Tresse, L., & Maddox, S.J., 1999, MNRAS, in press
- [9] Saunders, W., Rowan-Robinson, M. & Lawrence, A., 1992, MNRAS, 258, 134

- [10] Telles, E., Maddox, S., 1999, submitted to MNRAS
- [11] Tresse, L., Maddox, S.J., Loveday, J., & Singleton, C., 1999, MNRAS, in press
- [12] Zucca, E., et al., 1997, A&A, 326, 477